Supplementary Information
for

In-situ formation of CeO_2 coupled with hollow NiCo-LDH nanosheets for efficient photocatalytic hydrogen evolution

Qingyi Liu,‡[a] Guoying Tan,‡[a] Yu Long,[a] Jiaxu Wei,[a] Hao Tian,[a] Shiyu Xie[a] and Yu Tang*[a,b]

[a] State Key Laboratory of Applied Organic Chemistry, Key Laboratory of Nonferrous Metal Chemistry and Resources Utilization of Gansu Province, College of Chemistry and Chemical Engineering, Lanzhou University, Lanzhou 730000, P.R. China. E-mail: tangyu@lzu.edu.cn

[b] State Key Laboratory of Baiyunobo Rare Earth Resource Researches and Comprehensive Utilization, Baotou Research Institute of Rare Earths, Baotou 014030, P. R. China

‡ These authors contributed equally to this work.

Contents

1. Experimental Section

1.1 Chemicals

Nickel nitrate hexahydrate ($Ni(NO_3)_2·6H_2O$, 98%), cobalt nitrate hexahydrate ($Co(NO_3)_2·6H_2O$, 99%), cerium nitrate hexahydrate ($Ce(NO_3)_3·6H_2O$, 99.5%), 2-methylimidazole (2-MIM) ($C_4H_6N_2$, 97%), Eosin Y (EY, $C_{20}H_6Br_4Na_2O_5$), Tterephthalic acid (TA, $C_8H_6O_4$) , anhydrous methanol, anhydrous ethanol, dimethyl formamide (DMF) and triethanolamine (TEOA) were all commercially available and used directly without further purification.

1.2 Materials preparation

Synthesis of NiCo-layered double hydroxide nanosheets (NiCo-LDH NSs)

Typically, $Co(NO_3)_2·6H_2O$ (0.586 g, 2 mmol) was dissolved in methanol (20 mL) in a 100 mL round-bottom flask. Then, 6.7 mL of methanol solution with 2-MIM (0.616 g, 7.5 mmol) was quickly poured into the above solution under agitation. When the reaction system was heated to 90 °C, 10 mL of methanol solution of $Ni(NO_3)_2·6H_2O$ (0.32 g, 1.1 mmol) was added. After continuing the reaction for 2 hours, the mixture was transferred into a Teflon-lined stainless autoclave containing 30 mL of methanol. The mixture was then maintained at 120 °C for 2 hours, with both heating and cooling being performed in a programmed manner. Subsequently, the product was collected by centrifugation, washed several times with water and ethanol, and finally dried at 70 °C overnight.

Synthesis of CeO_2-coupled NiCo-layered double hydroxide nanosheets (NiCo-LDH/CeO_2 NSs)

The synthesis of NiCo-LDH/CeO_2 NSs was similar to that of NiCo-LDH NSs, except that $Ni(NO_3)_2·6H_2O$ was partially replaced by $Ce(NO_3)_3·6H_2O$ (86 mg, 0.2 mmol). The NiCo-LDH/CeO_2-2 NSs were synthesized by doubling the concentration of the reaction system. Samples with different Ce additions (0.1 mmol, 0.3 mmol) were also synthesized.

Synthesis of rare earth-doped NiCo-layered double hydroxide nanosheets (NiCo-LDH/RE NSs)

NiCo-LDH/RE nanosheets were synthesized with $Y(NO_3)_3·6H_2O$, $La(NO_3)_3·6H_2O$, $Gd(NO_3)_3·6H_2O$ and $Tb(NO_3)_3·6H_2O$ instead of $Ce(NO_3)_3·6H_2O$.

Synthesis of CeO_2 nanoparticles (CeO_2 NPs)

CeO_2 NPs were synthesized in a similar procedure as NiCo-LDH/CeO_2 NSs, with the difference that $Ni(NO_3)_2 \cdot 6H_2O$ and $Co(NO_3)_2 \cdot 6H_2O$ were not added.

1.3 Characterization

The powder X-ray diffraction (PXRD) patterns were obtained by a MiniFlex600 diffractometer with Cu-Kα radiation. Fourier transform infrared (FTIR) spectra of the materials were recorded using a Nicolet 360 FTIR spectrometer within the 4000–400 cm^{-1} wavenumber range. The sample composition was determined by an inductively coupled plasma optical emission spectroscopy (ICP-OES, Plasma Quant PQ9000). The diffuse reflection spectra of the samples were measured by UV-vis spectrophotometer (Shimadzu UV-2600) using $BaSO_4$ as reference. The Barrett-Emmett-Teller (BET) measurements were conducted on an ASAP 2020 Micropore Physisorption Analyzer. The scanning electron microscope (SEM) and transmission electron microscope (TEM) images were acquired by S-4800 (Hitachi, Japan) and Tecnai F30 (FEI, USA), respectively. X-ray photoelectron spectroscopy (XPS) spectra were performed by a Kratos Axis Supra device (SHIMADZU, Japan). Raman spectra were measured in a Lab Ram HR Evolution (HORIBA Jobin Yvon, France) with a 532 nm laser. The thickness of the nanosheets was measured by atomic force microscope (AFM) using a Dimension Icon (Bruker, USA). The photoluminescence (PL) spectra and time-resolved photoluminescence (TRPL) spectra were collected by a FluoroLog-3 fluorescence spectrometer (HORIBA, USA). A Zeta potential and particle size analyzer (90Plus PALS) was used to analyze Zeta potential. Electron paramagnetic resonance (EPR) spectra were operated on ER200DSRC10/12 (Bruker, Germany).

1.4 Photocatalytic hydrogen evolution experiment

The photocatalytic H_2 evolution experiment was performed on Labsolar-6A system (Beijing Perfectlight Technology Co., Ltd.). Typically, the 10 mg photocatalyst and 20 mg EY were dispersed in 30 mL TEOA solution (10 vol %), and then transferred to a 300 mL quartz reactor. After removing oxygen from the reactant system by vacuuming, the solution was irradiated by a 300 W Xe lamp ($\lambda \geq 400$ nm) as the light source while magnetic stirring was performed. The temperature of the reaction system was maintained by connecting the low temperature thermostat bath. The generated H_2 was analyzed periodically during the reaction by means of a gas chromatograph (GC9790

II) equipped with a thermal conductivity detector (TCD) and using high purity nitrogen as carrier gas.

1.5 Photoelectrochemical measurements

The photoelectrochemical measurements were conducted with a standard three-electrode system, in which a platinum plate and a saturated calomel electrode (SCE) were used as counter electrode and reference electrode, respectively, and the FTO glass coated with sample was used as working electrode. The working electrode was prepared as follows. Firstly, 5.0 mg electrocatalyst was dispersed in 400 μL DMF and 100 μL Nafion solution (5.0 wt%), and the suspension was treated by ultrasound for 1 hour. Afterwards, 50 μL catalyst ink was dropped onto the conductive surface of FTO glass in five installments using a pipette, followed by naturally drying in air. The electrolyte was 0.2 mol L^{-1} Na_2SO_4 aqueous solution and the geometrical surface area of working electrode immersed in the electrolyte was about 1 cm^2. Linear sweep voltammetry (LSV) measurements were conducted at a scan rate of 5 mV s^{-1} from −0.1 to −0.65 V vs SCE. Electrochemical impedance spectroscopy (EIS) measurements were performed with an amplitude of 5 mV, a quiet time of 2 s, and the frequency range from 0.1 Hz to 100 kHz. All tests were carried out on a CHI 760E electrochemistry workstation (Shanghai Chenhua, China).

1.6 Hydroxyl radical experiment

20 mg of catalyst was dispersed in 20 mL of mixed solution (0.02 M TA, 0.1 M NaOH), irradiated with a 300 W xenon lamp, and 3 mL of solution was taken every 15 min. The fluorescence test (excitation at 315 nm) was performed on clear solution after filtration.

1.7 Density functional theory (DFT) calculation

AIMD model

The AIMD model: $Ce(NO_3)_3 \cdot 6H_2O$, methyl alcohol, imidazole as the solution. The NiCo-LDH fragments are used as seed crystal. It is randomly distributed in 15.1 Å * 9.01 Å * 20.44 Å cells and the number of atoms is 236. In the initial state, the distance between various components is greater than 2.5 Å.

Calculation methodology

The density functional theory (DFT) implementation in CP2K/Quickstep [1] is based on a hybrid Gaussian plane wave (GPW) scheme, the orbitals are described by an atom centered Gaussian-type basis set, and an auxiliary plane wave basis set is used to re-expand the electron density in the reciprocal space. A matrix Orbital Transformation procedure was used for the wave function optimization. The 1s electrons of H, 2s, 2p electrons of C, 2s, 2p electrons of O, 2s, 2p electrons of N, 3s, 3p, 3d, 4s electrons of Ni, 3s, 3p, 3d, 4s electrons of Co, 5s, 5p, 4f, 5d, 6s electrons of Ce were treated as valence, and the rest core electrons were represented by Goedecker-Teter-Hutter (GTH) pseudopotentials [2,3].The Gaussian basis set was double- ζ with one set of polarisation functions (DZVP) [4], and the plane wave cutoff was set to 400 Ry. Perdew-Burke-Ernzerhof (PBE) functional [5] was used to describe the exchange correlation effects, and the dispersion correction was applied in all calculations with the Grimme D3 method [6]. In structure optimization, the geometries were optimized by Broyden-Fletcher Goldfarb-Shanno (BFGS) minimizer. For the heterojunction formation process, Ab-Initio Molecular Dynamics (AIMD) was employed, and canonical ensemble (NVT) conditions were imposed by a Nose-Hoover thermostat with a target temperature of 400 K. The MD time step is set to 0.5 fs. For all the MD trajectories, the initial ~ 0.2 ps (400 steps) was regarded as the equilibration period, and then followed by production periods of more than 6.0 ps.

All static calculations were carried out using spin-polarized density functional theory (DFT) corrections were carried out with the projector augmented wave (PAW) method using the Vienna Ab-initio Simulation Package (VASP) [6,7].

The exchange and correlation energy density functions were described by the Generalized Gradient Approximation (GGA) of Perdew-Burke-Ernzerh (PBE) [8,9]. To describe the correlation for 3d transition metal systems, the DFT+U method was used and the value of U was 3.4 for Co, 3.0 for Ni and 6.0 for Ce. The cutoff energy for plane-wave basis function was chosen to be 450 eV. The maximum force and energy change of 0.02 eV/Å and 10^{-5} eV, respectively. The 3 × 3 × 1 Monkhorst-Pack type of K-point set up was used for all surface structural models. Choose (100) surface of NiCo-LDH and (111) surface of CeO_2 and build a heterojunction structure of both. And the vacuum layer set to 18 Å.

The work function can be estimated using the line-up potential, and the work function ϕ is generally estimated as $\phi = E_{vac} - E_F$, where E_{vac} is the vacuum level, E_F is the Fermi energy, and ΔV is the difference between average potentials along the c direction residing in CeO_2 and NiCo-LDH regions.

2. Supporting Figures

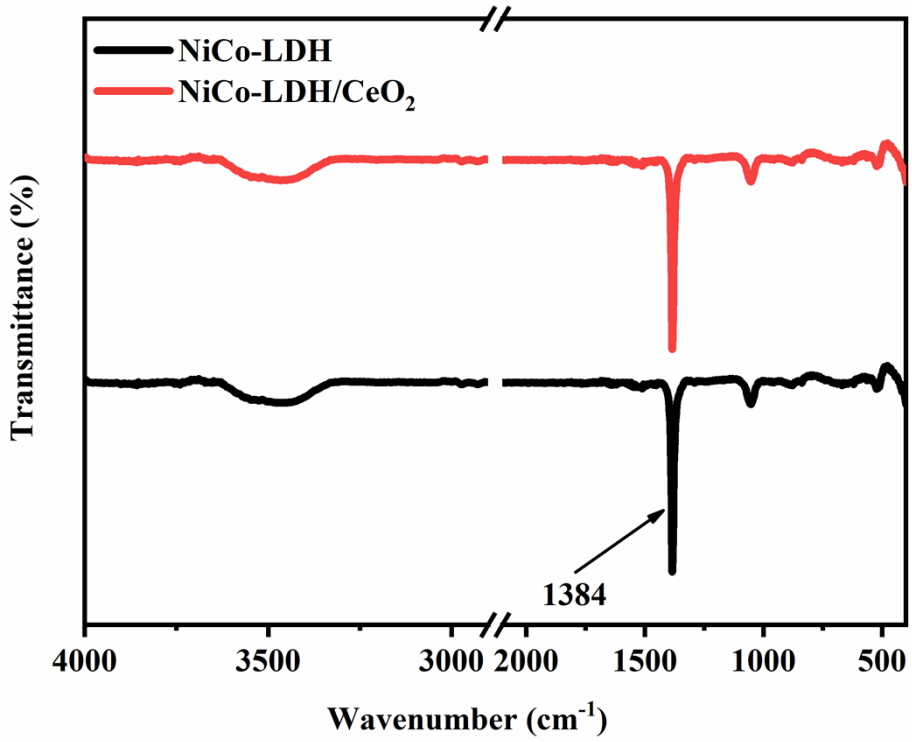

Fig. S1. FTIR spectra of NiCo-LDH NSs and NiCo-LDH/CeO_2 NSs.

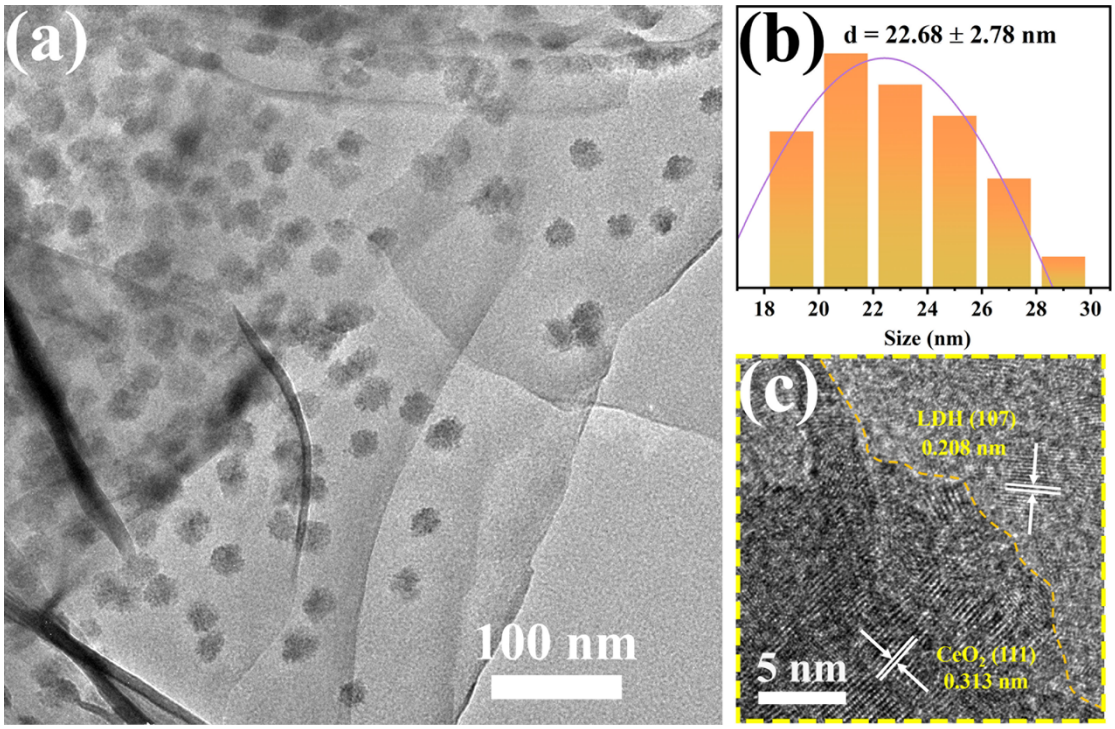

Fig. S2. (a) TEM, (c) HRTEM images of NiCo-LDH/CeO_2 NSs, (b) the histogram of size distribution of CeO_2 nanoparticles on NiCo-LDH/CeO_2 NSs

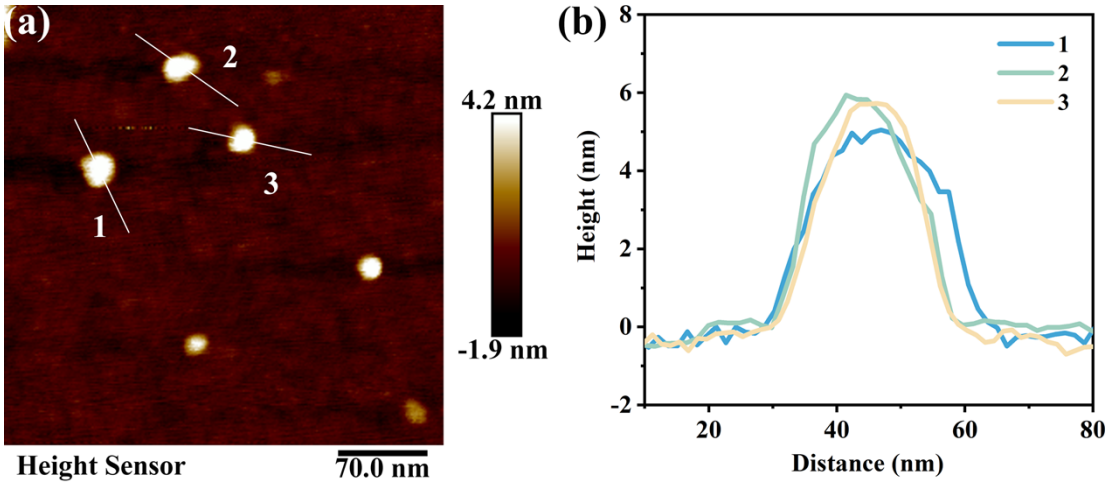

Fig. S3. (a) AFM image of NiCo-LDH/CeO_2 NSs and (b) the corresponding height profile.

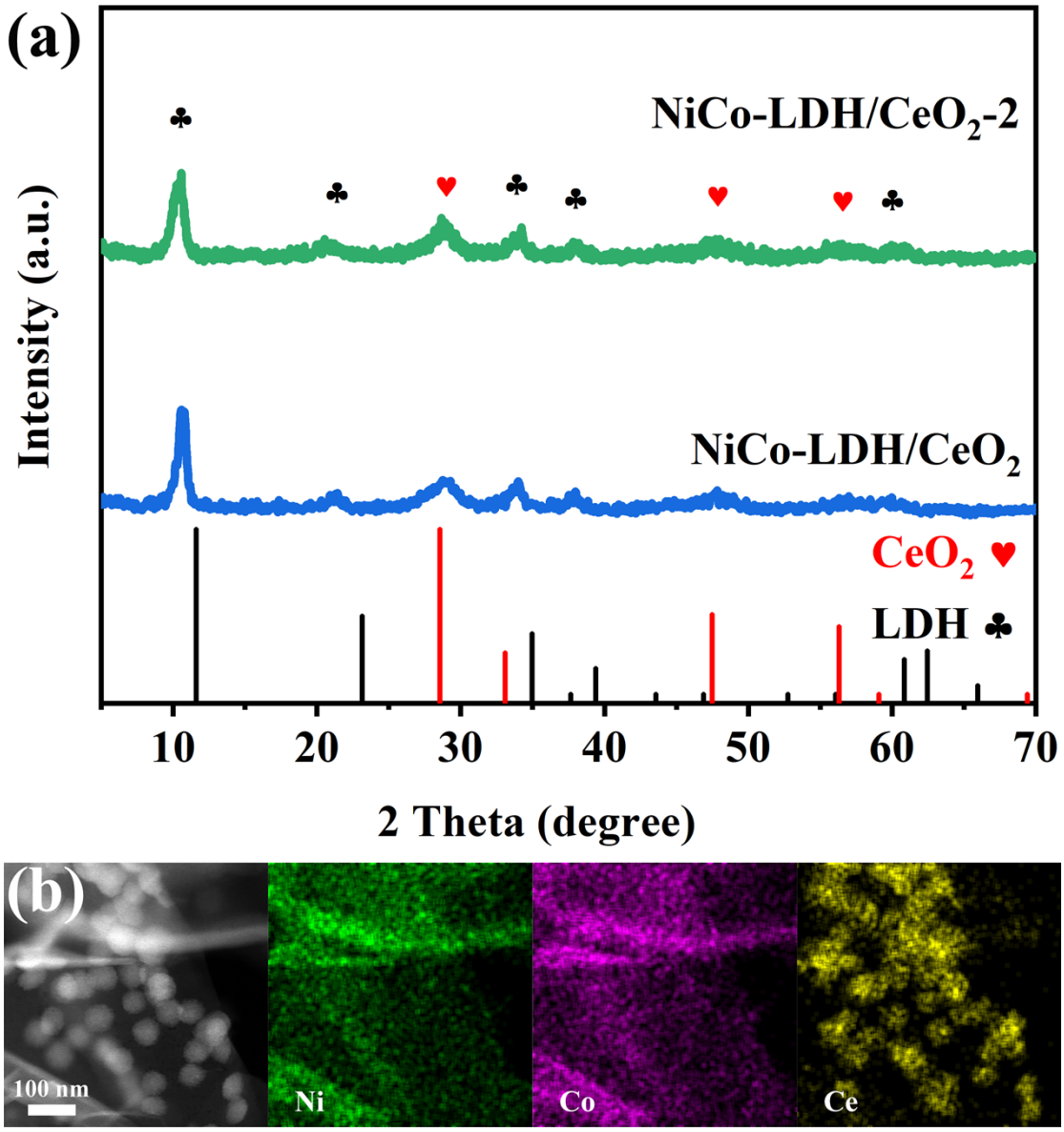

Fig. S4. (a) XRD spectra of NiCo-LDH/CeO_2-2 NSs and NiCo-LDH/CeO_2 NSs, (b) the elemental mapping images of NiCo-LDH/CeO_2-2 NSs.

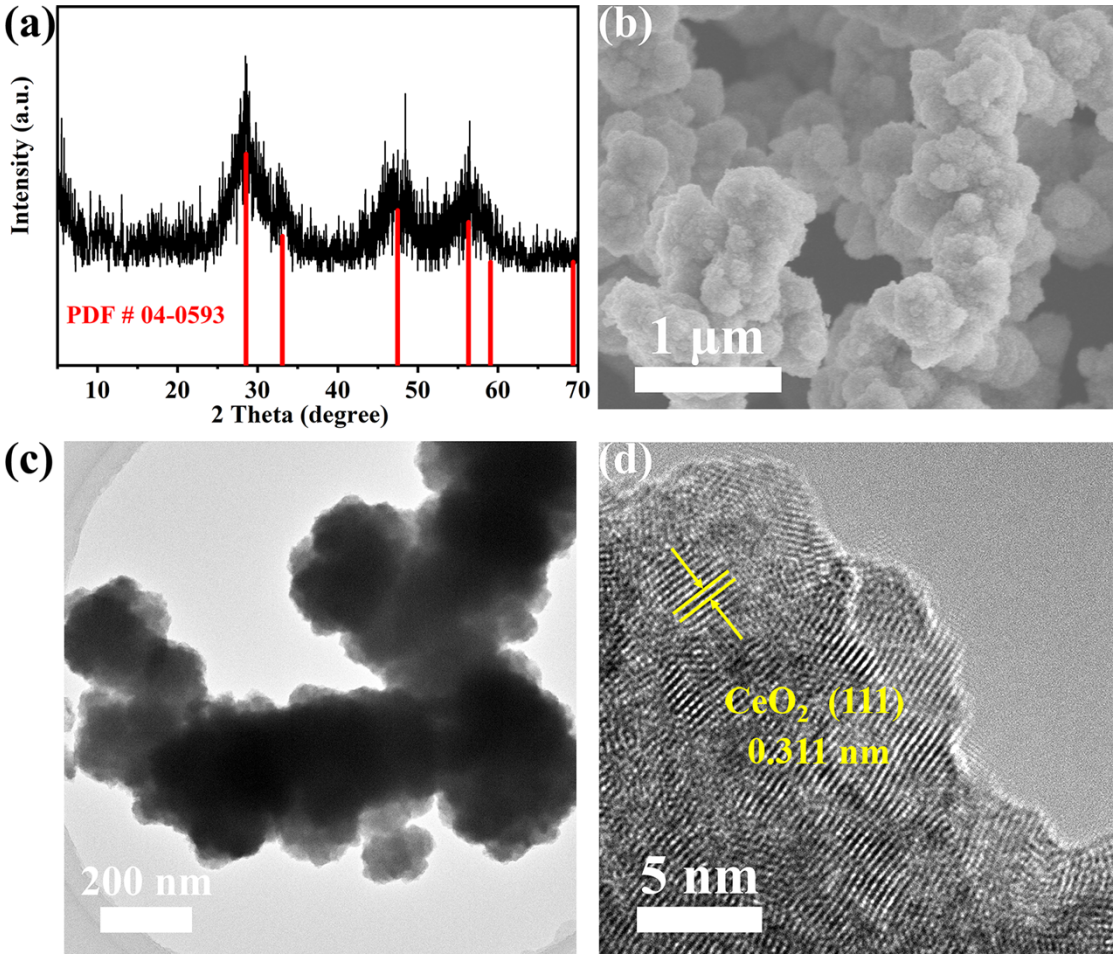

Fig. S5. (a) XRD spectrum, (b) SEM, (c) TEM and (d) HRTEM images of CeO_2 NPs.

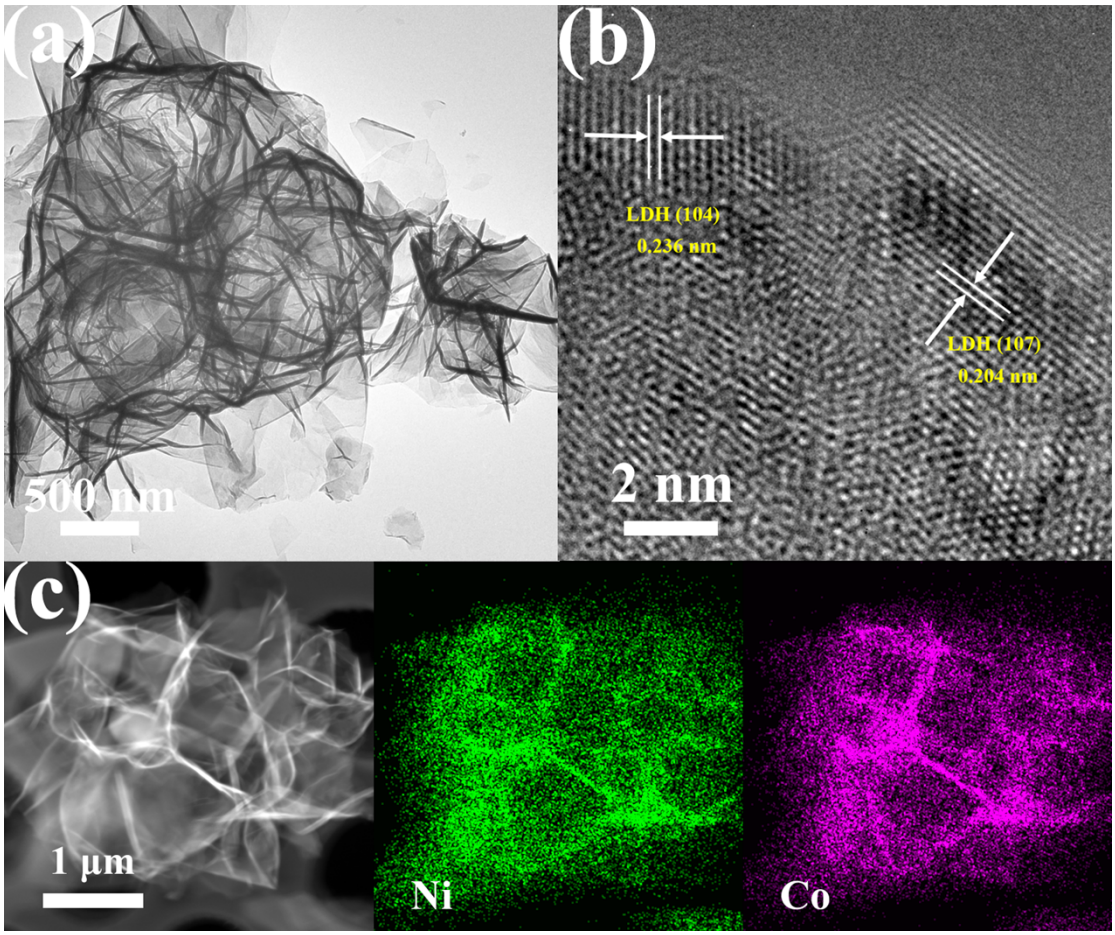

Fig. S6. (a) TEM, (b) HRTEM, and (c) HAADF-STEM and the corresponding element mapping images of NiCo-LDH NSs.

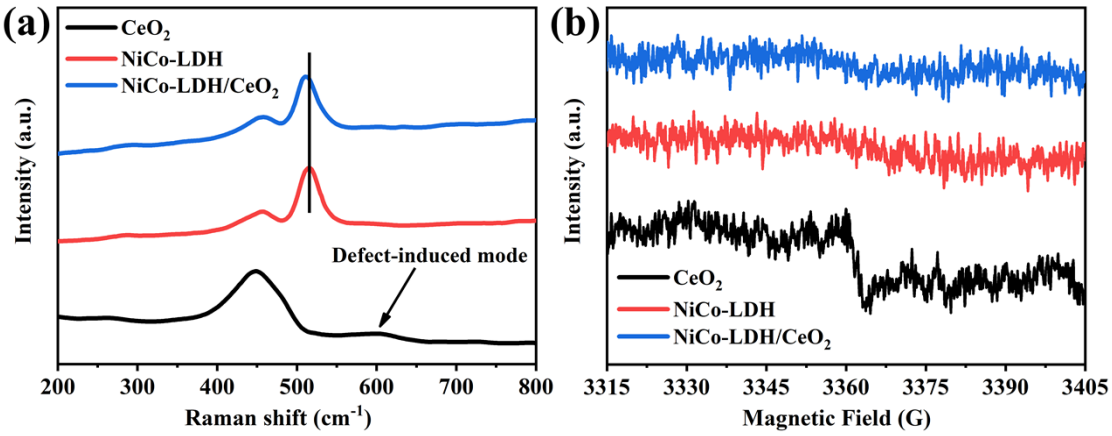

Fig. S7. (a) Raman spectra and (b) EPR spectra of CeO_2 NPs, NiCo-LDH NSs and NiCo-LDH/CeO_2 NSs.

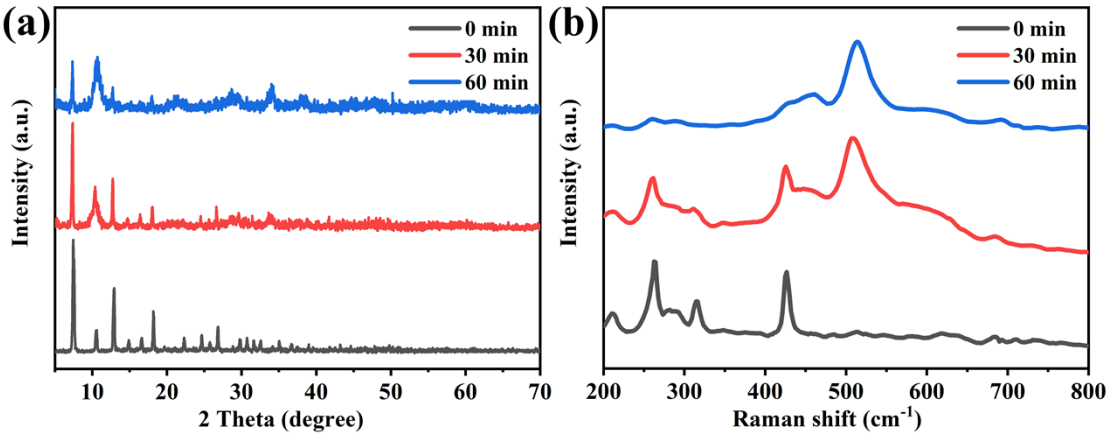

Fig. S8. (a) XRD spectra and (b) Raman spectra of the products after different reaction time.

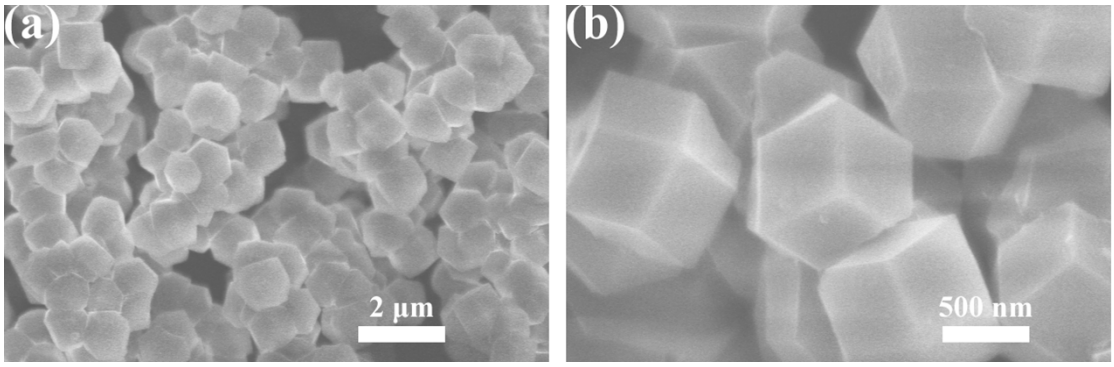

Fig. S9. SEM images of ZIF-67.

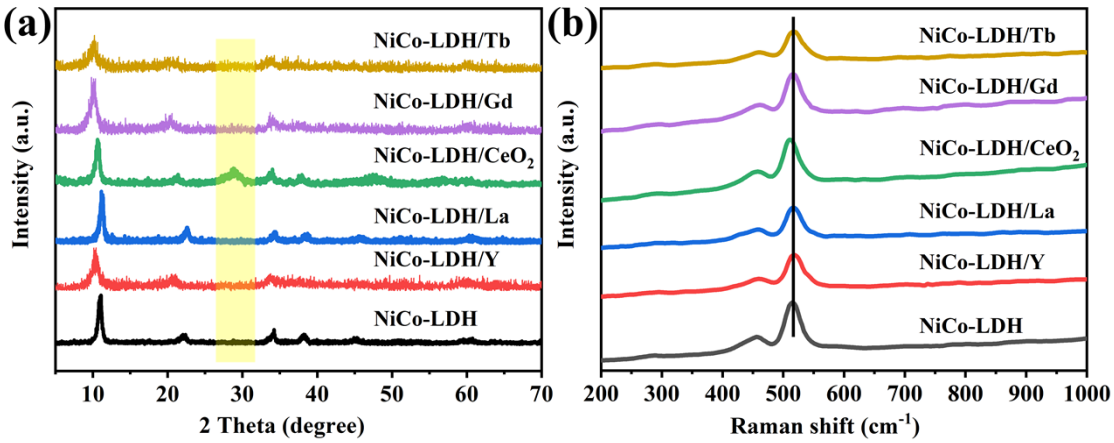

Fig. S10. (a) XRD patterns and (b) Raman spectra of NiCo-LDH NSs, NiCo-LDH/Y NSs, NiCo-LDH/La NSs, NiCo-LDH/CeO_2 NSs, NiCo-LDH/Gd NSs and NiCo-LDH/Tb NSs.

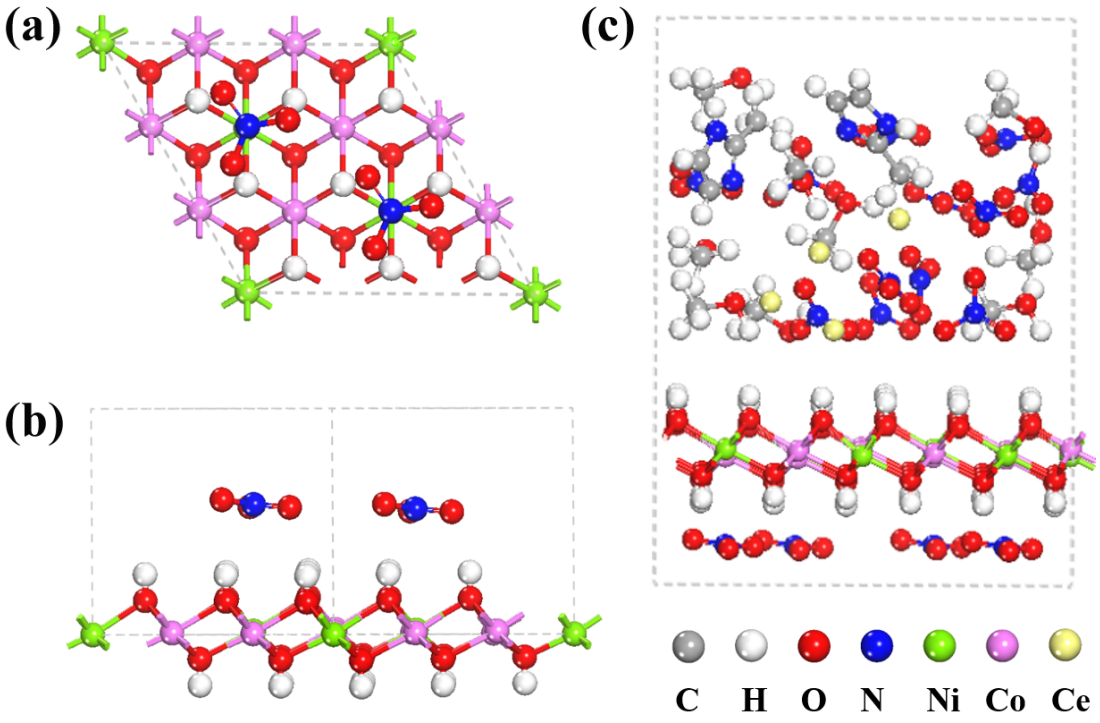

Fig. S11. (a–b) Optimization models of NiCo-LDH along different directions. (c) The solid-liquid model for kinetic calculation.

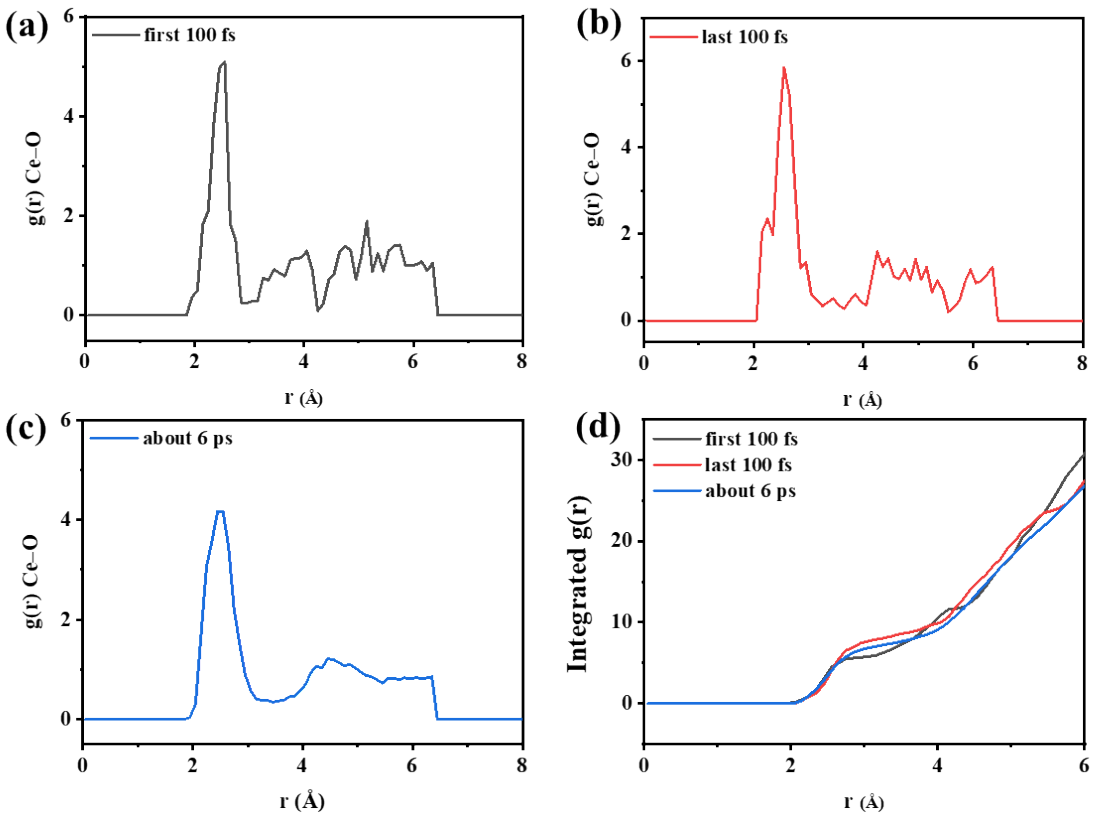

Fig. S12. (a–c) Radial distribution function at different times. (d) The first coordination layer from integrating radial functions.

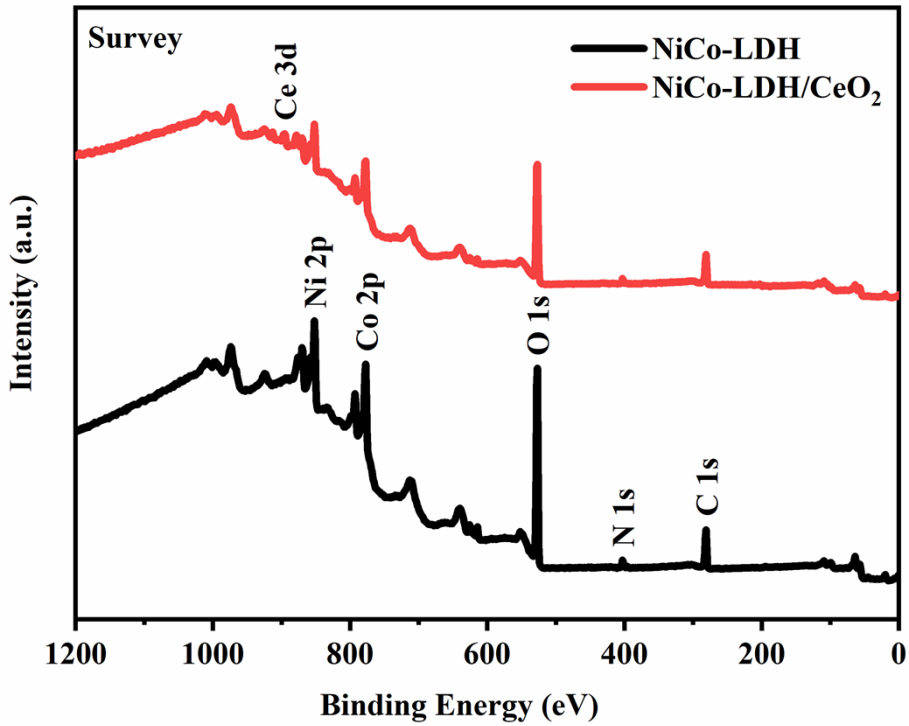

Fig. S13. XPS survey spectra of NiCo-LDH NSs and NiCo-LDH/CeO_2 NSs.

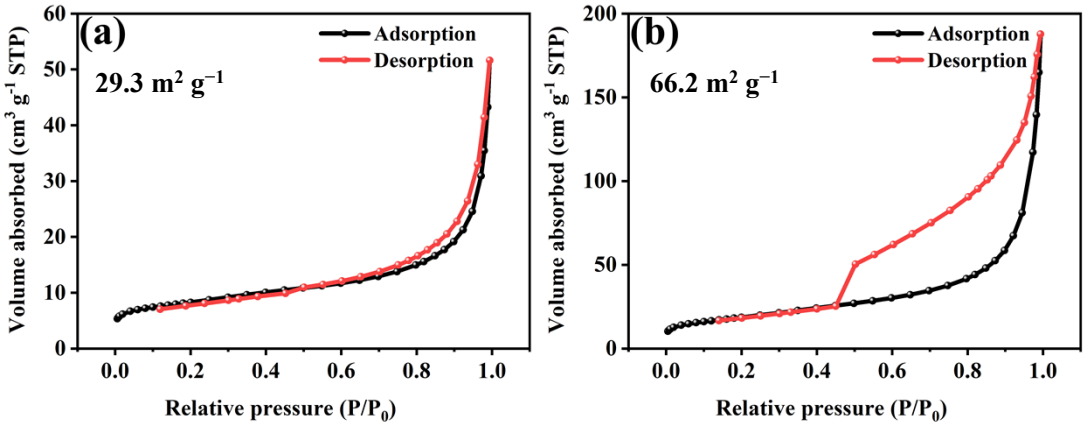

Fig. S14. N_2 adsorption (black)/desorption (red) isotherms of (a) NiCo-LDH NSs and (b) NiCo-LDH/CeO_2 NSs.

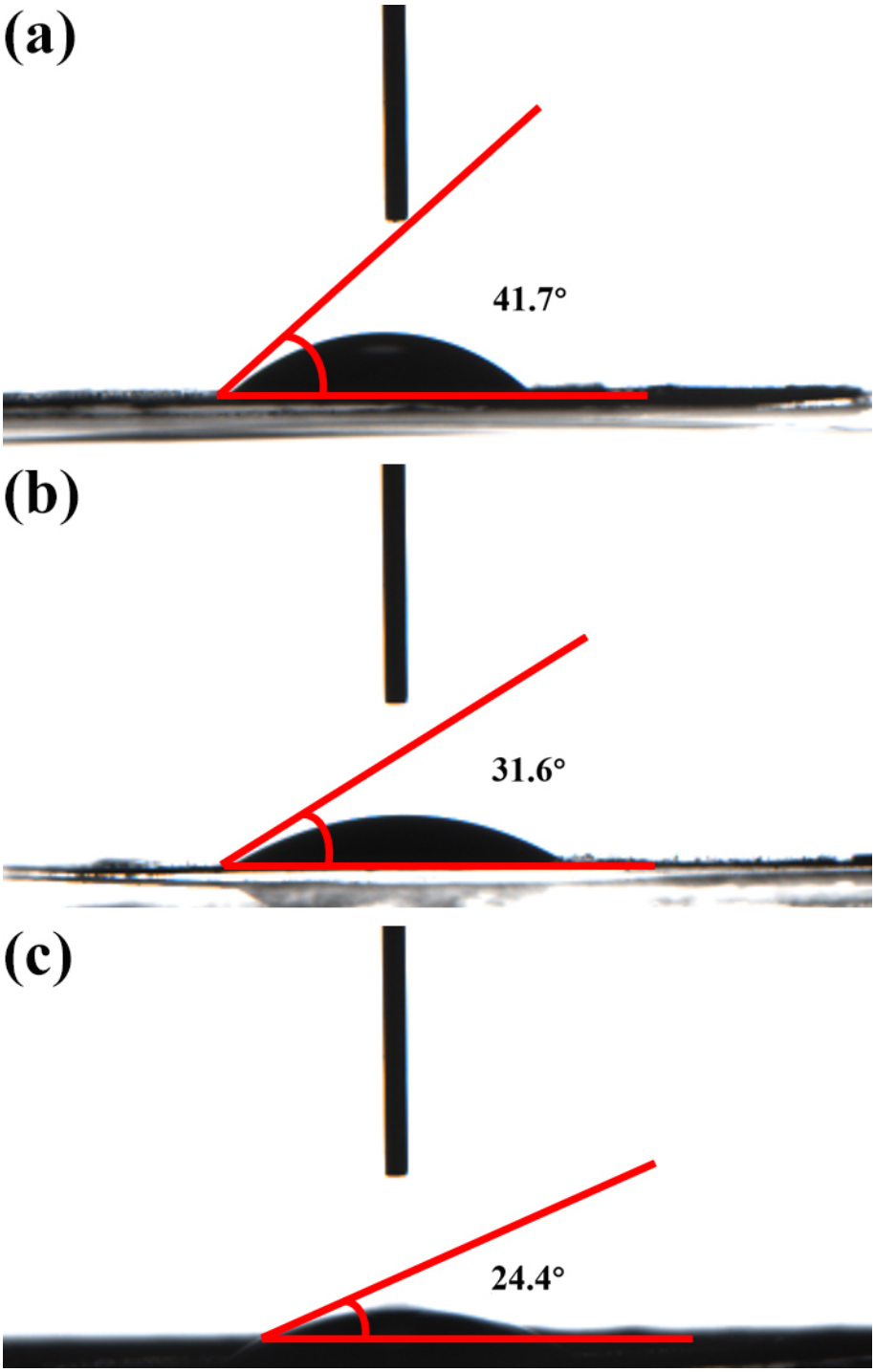

Fig. S15. Water contact angles of (a) CeO_2 NPs, (b) NiCo-LDH NSs and (c) NiCo-LDH/CeO_2 NSs.

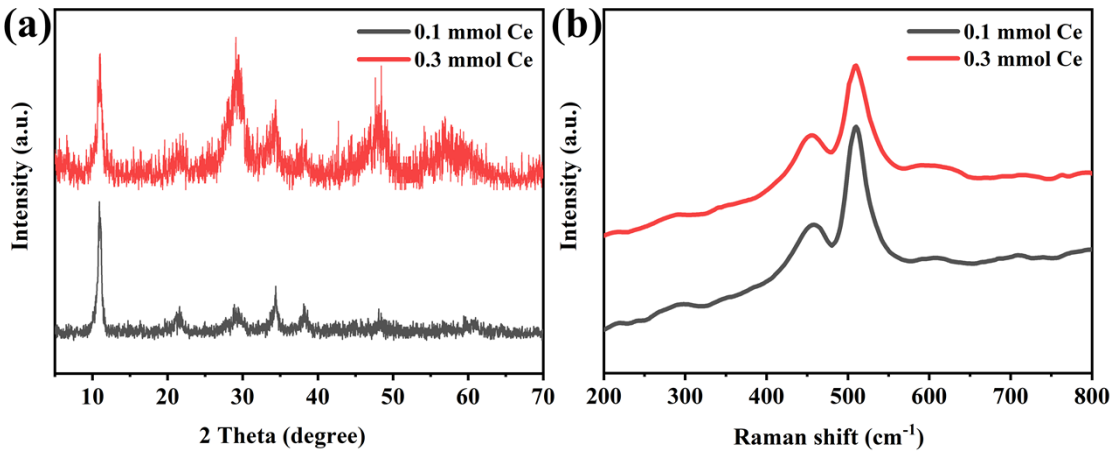

Fig. S16. (a) XRD spectra and (b) Raman spectra of the samples with different Ce additions.

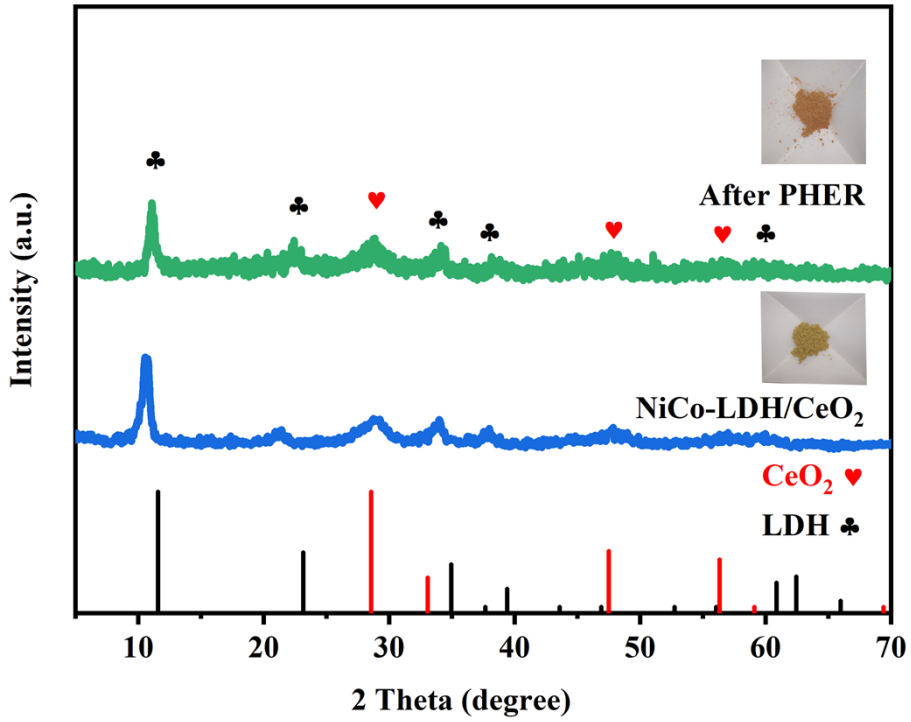

Fig. S17. XRD pattern of NiCo-LDH/CeO_2 NSs before and after PHER (the insets are photographs of the samples before and after the reaction).

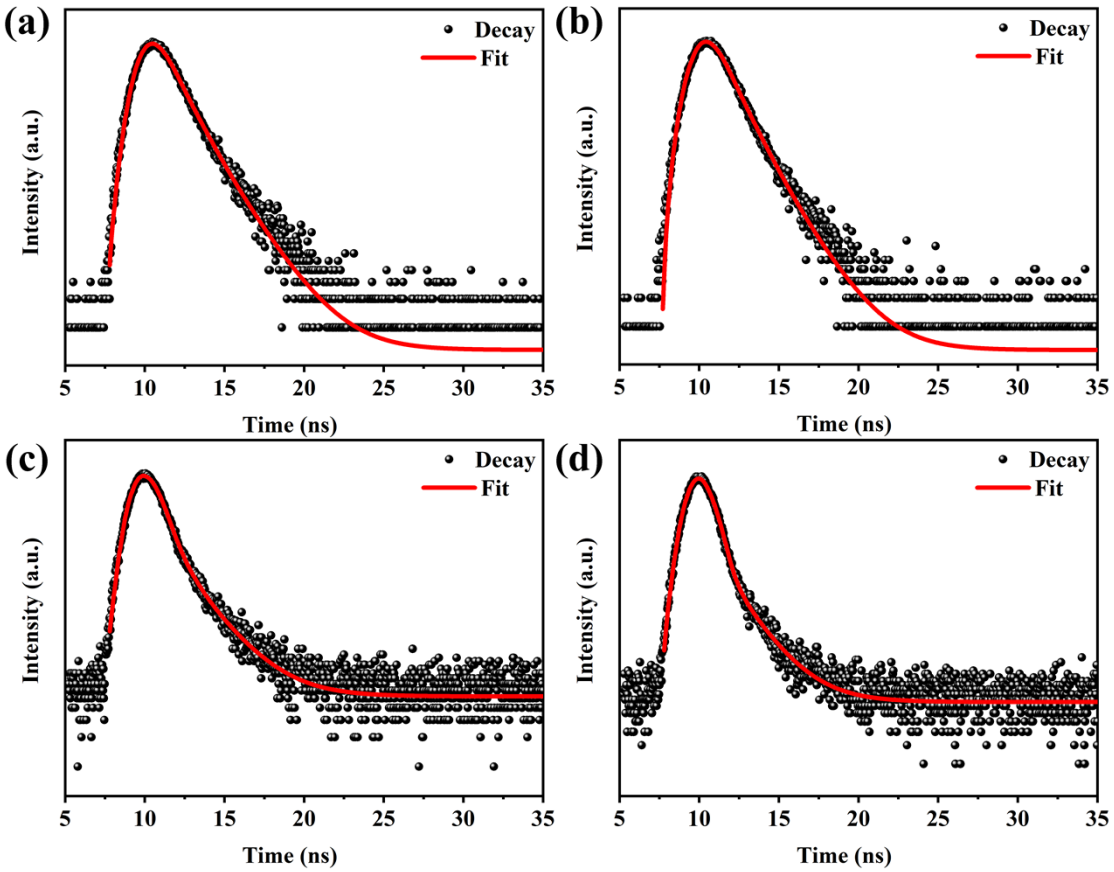

Fig. S18. The fluorescence decay and fitting curves of (a) EY, (b) CeO_2 NPs, (c) NiCo-LDH NSs, and (d) NiCo-LDH/CeO_2 NSs with the emission monitored at 537 nm (λ_{ex} = 455 nm).

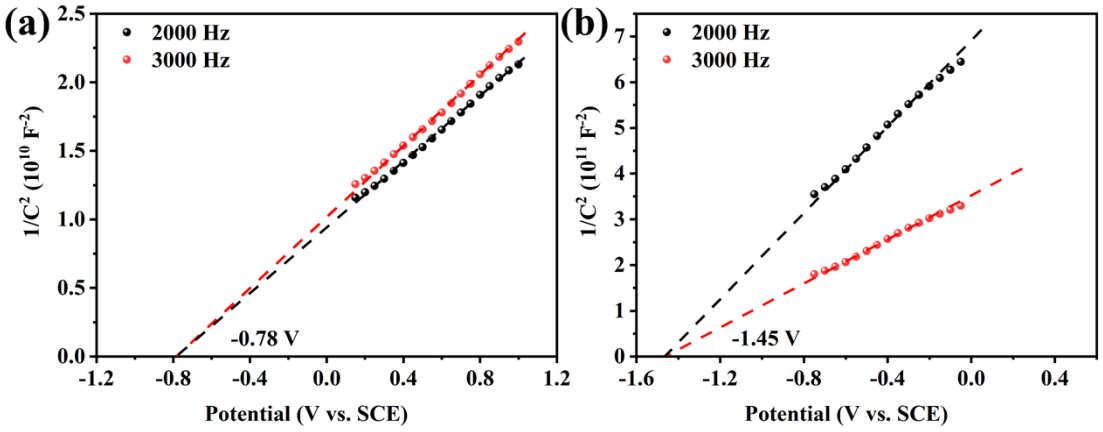

Fig. S19. Mott-Schottky plots of (a) CeO_2 NPs and (b) NiCo-LDH NSs.

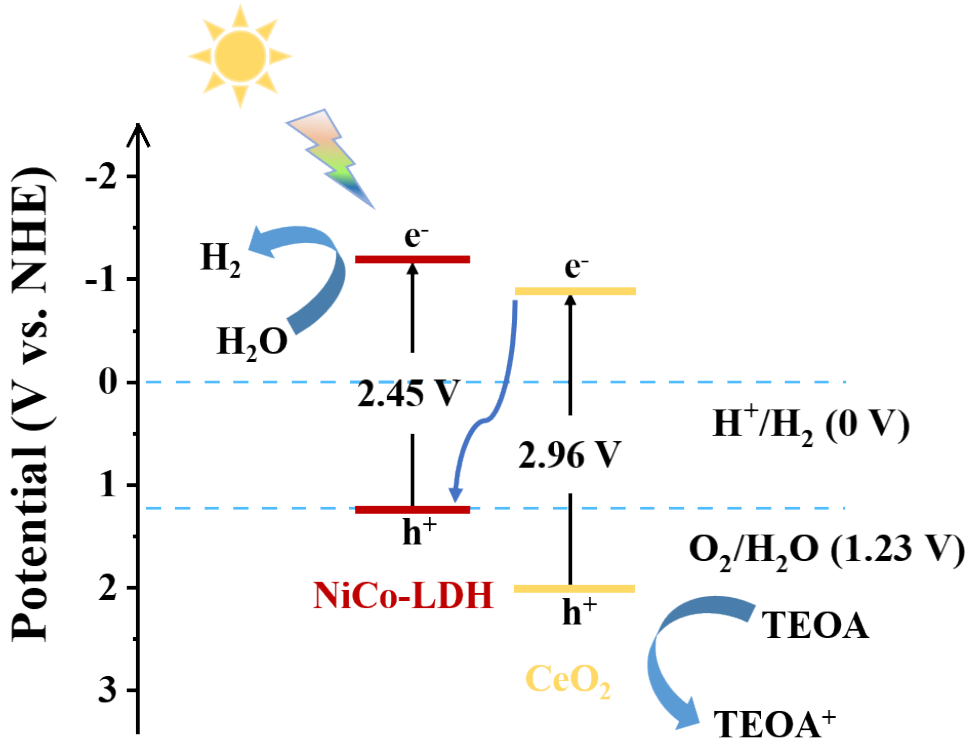

Fig. S20. Possible Z-scheme heterojunction between CeO_2 and NiCo-LDH.

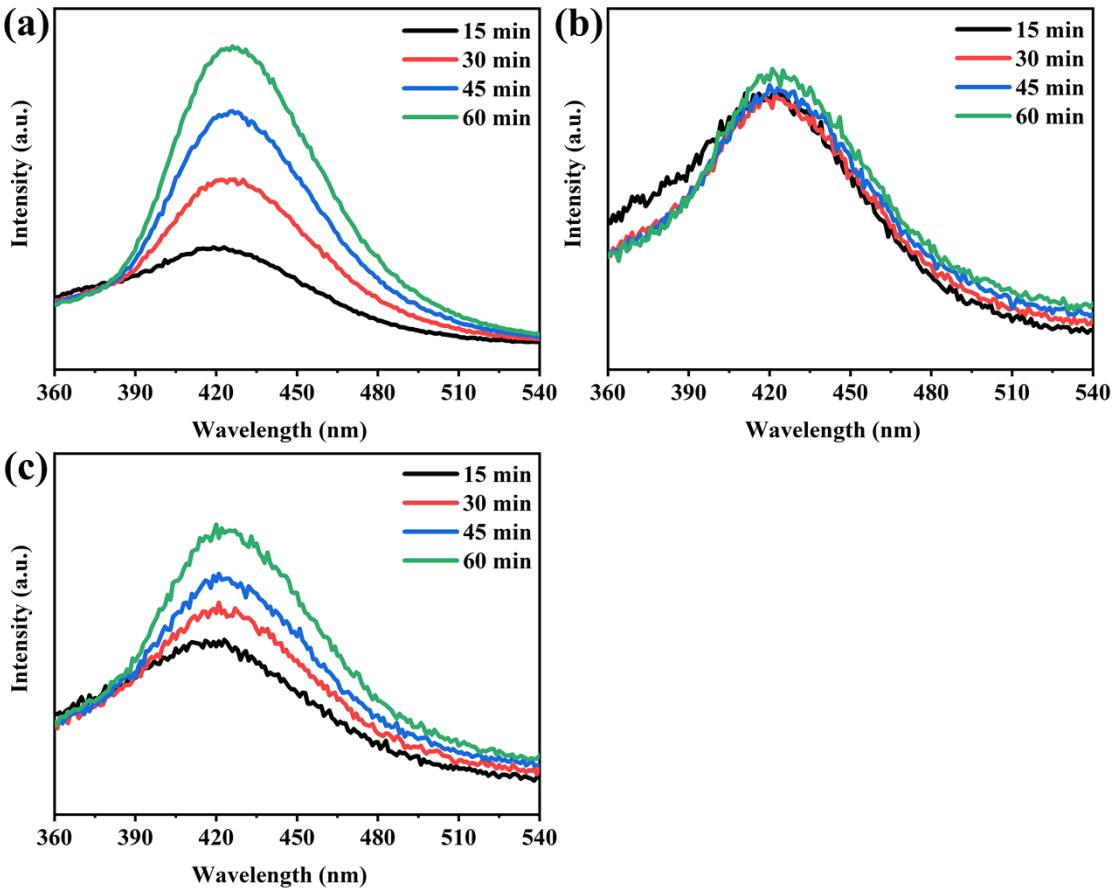

Fig. S21. Photoluminescence spectra of (a) CeO_2 NPs, (b) NiCo-LDH NSs and (c) NiCo-LDH/CeO_2 NSs during reaction process with TA under illumination (λ_{ex} = 315 nm).

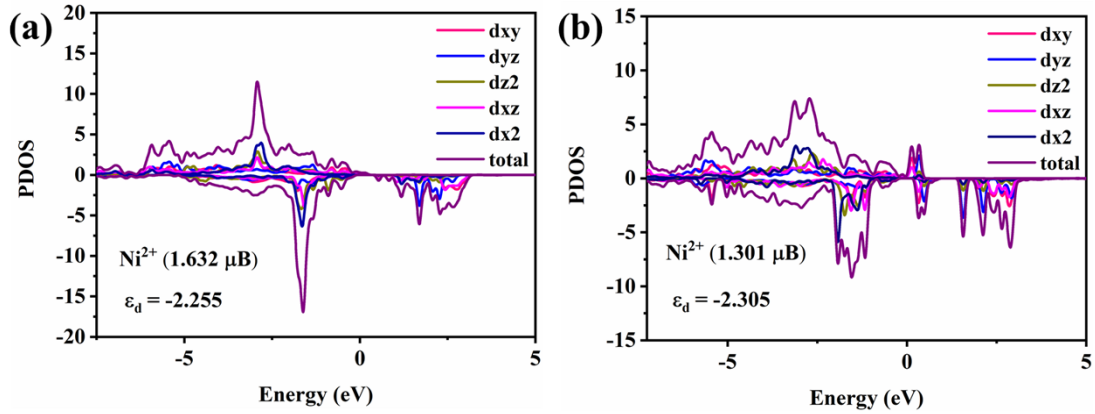

Fig. S22. Partial density of states (PDOS) of (a) NiCo-LDH/CeO_2, (b) NiCo-LDH.

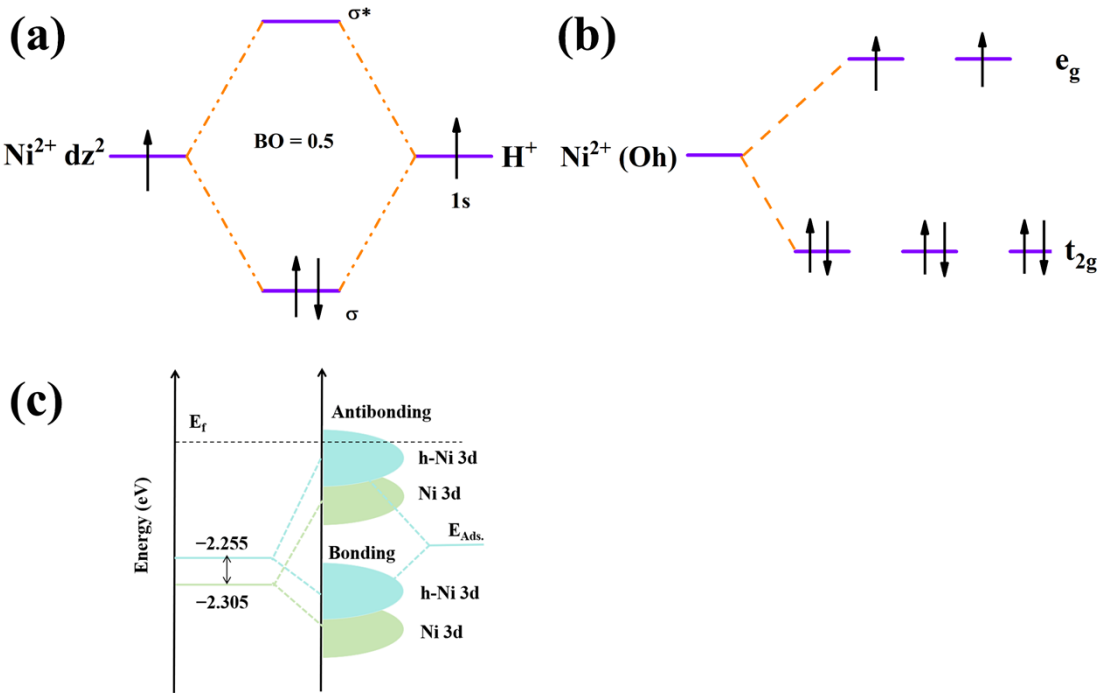

Fig. S23. (a) The orbital interactions between Ni^{2+} and PHER intermediates (*H). (b) Geometrically spin orientations of Ni^{2+} (Oh). (c)The corresponding schematic illustration of bond formation between the reaction surface and the adsorbate (the h represents heterojunction).

3. Supporting Tables

Table S1. Comparison of PHER performance with LDH-based photocatalysts reported in the literature.

Photocatalysts	Sacrificial agent	Light source	Hydrogen evolution rate ($\mu mol\ g^{-1}\ h^{-1}$)	References
NiAl-LDH/CoS_x	TEOA solution	5W LED ($\lambda \geq 420nm$)	3678.6	*J. Colloid Interface Sci.* **2022**, *609*, 686–697
MgAl-LDH/NiS	20 vol % CH_3OH	300W Xe lamp ($\lambda \geq 420nm$)	895	*Appl. Surf. Sci.* **2020**, *506*, 144999
CuCdCe-LDH/g-C_3N_4	Na_2S/Na_2SO_3	420W Xe lamp	3500	*Int. J. Hydrog. Energy* **2022**, *47*, 40227–40241
NiCo-LDH/g-C_3N_4	10 vol % TEOA	300W Xe lamp ($\lambda \geq 420nm$)	755	*Int. J. Hydrog. Energy* **2023**, *48*, 16704–16714
NiCo-LDH/P-CdS	10 vol % Lactic acid	300W Xe lamp ($\lambda \geq 400nm$)	8665	*Appl. Catal. B* **2019**, *254*, 145–155
ZnS/Zn-In-LDH	0.1 M Na_2S and 0.1 M Na_2SO_4	300W Xe lamp ($\lambda \geq 400nm$)	49.3	*Appl. Catal. B* **2021**, *292*, 120187
H-PBA@D-LDH	10 vol % Lactic acid	300W Xe lamp	260.3	*Chem. Eng. J.* **2023**, *475* 146062
CeO_2/CoAl-LDH	15 vol % TEOA	5W Xe lamp ($\lambda \geq 400nm$)	1231.4	*Surf. Interfaces* **2021**, *24* 101105
ZIS@Ni−Fe LDH	10 vol % TEOA	300W Xe lamp ($\lambda \geq 420nm$)	2035.8	*Inorg. Chem.* **2021**, *60*, 9762−9772
NiAl-LDH/NiS	15 vol % TEOA	5W LED	3408	*ACS Appl. Energy Mater.* **2022**, *5*, 8157−8168
2D-C_3N_4/NiFe-LDH	10 vol % TEOA	450 W solar simulator with an AM 1.5G filter	3087	*ACS Appl. Mater. Interfaces* **2021**, *13*, 24723−24733

NiFe-LDH/$Zn_{0.5}Cd_{0.5}S$	20 vol % Lactic acid	300W Xe lamp ($\lambda \geq 420$nm)	1017.6	*ACS Appl. Mater. Interfaces* **2021**, *13*, 39331−39340
NiCo-LDH/CeO_2	10 vol % TEOA	5 W LED	2700	*New J. Chem.* **2022**, *46*, 18408–18417
$CdIn_2S_4$@CoAl-LDH	10 vol % TEOA	300W Xe lamp ($\lambda \geq 420$nm)	793.4	*Inorg. Chem. Front.* **2022**, *9*, 994–1005
NiCo-LDH/CeO_2	**10 vol % TEOA**	**300W Xe lamp ($\lambda \geq 400$nm)**	**4312**	**This work**

Table S2. The zeta potentials of EY, CeO_2, NiCo-LDH, and NiCo-LDH/CeO_2.

Samples	Test 1 (mV)	Test 2 (mV)	Test 3 (mV)	Average (mV)
EY	**−54.18**	**−53.48**	**−52.72**	**−53.46**
CeO_2	**9.55**	**9.02**	**9.61**	**9.39**
NiCo-LDH	**21.49**	**21.61**	**22.77**	**21.96**
NiCo-LDH/CeO_2	**26.4**	**27.09**	**27.47**	**26.99**

Table S3. The decay lifetimes of EY, CeO_2, NiCo-LDH, and NiCo-LDH/CeO_2.

Samples	τ_1 (ns)	τ_2 (ns)	τ_{av} (ns)
EY	1.09	1.92	1.25
CeO_2	1.07	1.85	1.19
NiCo-LDH	0.61	2.03	0.78
NiCo-LDH/CeO_2	0.38	1.86	0.47

References

[1] VandeVondele, J. et al. Quickstep: Fast and accurate density functional calculations using a mixed Gaussian and plane waves approach. Comput. Phys. Commun. 167, 103–128, (2005).

[2] Goedecker, S., Teter, M. & Hutter, J. Separable dual-space Gaussian pseudopotentials. Phys. Rev. B 54, 1703–1710, (1996).

[3] Hartwigsen, C., Goedecker, S. & Hutter, J. Relativistic separable dual-space Gaussian pseudopotentials from H to Rn. Phys. Rev. B 58, 3641–3662, (1998).

[4] Vandevondele, J. & Hutter, J. Gaussian basis sets for accurate calculations on molecular systems in gas and condensed phases. J. Chem. Phys. 127, 114105, (2007).

[5] Perdew, J. P., Burke, K. & Ernzerhof, M. Generalized gradient approximation made simple. Phys. Rev. Lett. 77, 3865–3868, (1996).

[6] G. Kresse, J. Furthmüller, Efficiency of ab-initio total energy calculations for metals and semiconductors using a plane-wave basis set, Comp. Mater. Sci. 6 (1996) 15–20

[7] G. Kresse, J. Furthmüller, Efficient iterative schemes for ab initio total-energy calculations using a plane-wave basis set, Phys. Rev. B 54 (1996) 11169–11186

[8] P.E. Blöchl, Projector augmented-wave method, Phys. Rev. B 50 (1994) 17953

[9] G. Kresse, D. Joubert, From ultrasoft pseudopotentials to the projector augmented wave method, Phys. Rev. B 59 (1999) 1758–1775